Zn and Ni doping effects on the low-energy spin excitations in $La_{1.85}Sr_{0.15}CuO_4$

M. Kofu,[1,2,*] H. Kimura,[3] and K. Hirota[1]
[1]*Institute for Solid State Physics, University of Tokyo, Kashiwa 277-8581, Japan*
[2]*Department of Physics, Tohoku University, Sendai 980-8578, Japan*
[3]*Institute of Multidisciplinary Research for Advanced Materials, Tohoku University, Sendai 980-8577, Japan*
(Received 5 October 2004; revised manuscript received 8 June 2005; published 2 August 2005)

Impurity effects of Zn and Ni on the low-energy spin excitations were systematically studied in optimally doped $La_{1.85}Sr_{0.15}Cu_{1-y}A_yO_4$ (A=Zn,Ni) by neutron scattering. Impurity-free $La_{1.85}Sr_{0.15}CuO_4$ shows a "spin gap" of ω=4 meV below T_c in the antiferromagnetic incommensurate spin excitation. In Zn:y=0.004, the spin excitation shows a spin gap of 3 meV below T_c. In Zn:y=0.008 and Zn:y=0.011, however, the dynamical susceptibility χ'' at ω=3 meV decreases below T_c and increases again at lower temperature, indicating an *in-gap* state. In Zn:y=0.017, the low-energy spin state remains unchanged with decreasing temperature, and elastic magnetic peaks appear below ~20 K and then exponentially grow. These results suggest that Zn induces a novel in-gap spin state, which becomes dominant and more static with increasing Zn. As for Ni:y=0.009 and Ni:y=0.018, the low-energy excitations below ω=3 meV and 2 meV disappear below T_c. The temperature dependence of χ'' at ω=3 meV, however, shows no upturn in contrast with Zn:y=0.008 and Zn:y=0.011, indicating the absence of an in-gap state. In Ni:y=0.029, though the magnetic signals were observed also at ω=0 meV, they showed no temperature dependence, implying that there is no static component. Furthermore, as ω increases, the magnetic peak width broadens and the peak position shifts toward the magnetic zone center ($\pi\pi$). We interpret the impurity effects as follows: Zn locally makes a nonsuperconducting *island* exhibiting the in-gap state in the superconducting *sea* with the spin gap. Zn reduces the superconducting volume fraction, thus suppressing T_c. On the other hand, Ni primarily affects the superconducting sea, and the spin excitations become more dispersive and broaden with increasing energy, which is recognized as a consequence of the reduction of energy scale of spin excitations. We believe that the reduction of energy scale is relevant to the suppression of T_c.

DOI: 10.1103/PhysRevB.72.064502 PACS number(s): 74.72.Dn, 74.62.Dh, 74.25.Ha, 78.70.Nx

I. INTRODUCTION

In past years, a large number of neutron scattering studies have suggested that antiferromagnetic (AF) spin fluctuations are relevant to the mechanism of high-T_c superconductivity. Significant features of AF spin correlations in exhaustively studied $La_{2-x}Sr_xCuO_4$ (LSCO) and $YBa_2Cu_3O_{6+x}$ (YBCO) are summarized as follows: (i) A well-defined gap with a gap energy E_{sg} opens below the superconducting transition temperature T_c in the energy spectrum, which is often called the "spin gap." It is known that the spin gap is also probed by nuclear magnetic resonance (NMR) measurements of $1/T_1T$; the spin gap opens at T^* ($>T_c$), and T^* reported by NMR measurements is similar to that observed by inelastic neutron scattering in YBCO (Ref. 1) and LSCO (Ref. 2). As for LSCO, the spin gap is observed only around the optimum doping concentration $0.15 \leqslant x \leqslant 0.18$.[2–4] On the other hand, the spin gap of YBCO appears in the superconducting state and there exists a relationship $E_{sg} \propto T_c$ in the region $0.5 \leqslant x \leqslant 0.95$.[1,5] (ii) In both LSCO and YBCO, the spin excitations appear at incommensurate positions $Q=(\frac{1}{2} \pm \delta \frac{1}{2} 0)$, $(\frac{1}{2} \frac{1}{2} \pm \delta 0)$ in the high-temperature tetragonal (HTT) notation. Additionally, the incommensurability δ is proportional to T_c in LSCO ($x \leqslant 0.15$) (Ref. 6) and YBCO ($x \leqslant 0.6$) (Ref. 5). However, it is ambiguous whether the incommensurate peaks of LSCO and that of YBCO have the same origin.[7] For example, the incommensurate peaks of YBCO are not clearly separated due to the broadened peak. (iii) The magnetic excitation of YBCO is enhanced below T_c at a particular energy E_r ($\propto T_c$) and a position $Q=(\frac{1}{2} \frac{1}{2} l)$, which is called a magnetic resonance peak. The existence of the magnetic resonance peak in LSCO is still an open question.[8,9]

To study whether a certain phenomenon is related to the superconductivity, reducing T_c is very effective. There exist many ways for T_c reduction; for example, crystal structure, magnetic field, and impurity substitution. Impurity substitution for Cu sites can be chosen so as to affect a particular property; ions with a different valence change carrier doping rate in the CuO_2 plane, the ionic radius mismatch induces local distortions, and the spins of impurities affect magnetic correlations. Thus, we can control a particular parameter to investigate which parameter is most related to T_c. Substitutions by divalent transition metal ions for Cu sites conserve the carrier doping level and hardly influence on the macroscopic crystal structure, which is reflected in the changes of lattice constants and structural phase transition temperature. In particular, the nonmagnetic ion Zn^{2+} ($3d^{10}$,S=0) and magnetic ion Ni^{2+} ($3d^8$,S=1) are suitable to understanding how magnetic interaction contributes to the high-T_c pairing mechanism. It is known that the T_c-suppression effect of Zn is stronger than that of Ni, unlike those for BCS superconductors. Furthermore, magnetic susceptibility measurements show that local magnetic moments induced by Zn are larger than those by Ni.[10] NMR studies for YBCO indicate that there exist staggered moments on Cu sites around Zn,[11,12] suggesting that Zn induces local magnetic moments around

itself. In scanning tunneling microscopy (STM) studies for impurity-doped $Bi_2Sr_2CaCu_2O_{8+\delta}$ (Bi2212) near the impurity site, Zn induces an intense quasiparticle scattering resonance,[13] while Ni makes quasiparticle state near the superconducting gap.[14] These results indicate that effects of Zn on the superconductivity and the magnetism are different from those of Ni. For the study of impurity doping, we should choose a high-T_c superconductor of which the overall behaviors have already been revealed and which has a single CuO_2 layer in order to avoid the ambiguity for which Cu-site impurities are substituted. For this reason, LSCO is most suitable.

Systematic neutron scattering studies on impurity substitution have not been performed, because neutron scattering studies need large and homogeneous single crystals. It is even more difficult to prepare a single crystal with a correctly controlled impurity concentration. Recently, however, Kimura *et al.* have systematically studied Zn doping effects on the low-energy AF spin excitations for optimally doped $La_{1.85}Sr_{0.15}CuO_4$ with various Zn concentrations, through strenuous efforts for crystal growth.[15,16] They have revealed that Zn induces a novel AF spin state in the spin gap, which they call an *in gap* state. They also found that the induced state becomes more dominant and more static with increasing Zn. Combined with STM and muon spin relaxation (μSR) studies which suggest that the superconductivity is excluded around Zn,[13,17] they have concluded that the induced state appears in the nonsuperconducting region and that the induced-state regions are spatially separated from the superconducting regions which exhibit the spin-gap state.

In this paper, we report Zn and Ni doping effects on the low-energy AF spin excitations and the superconducting transition. Our purpose is to clarify the difference between the effects of Zn and those of Ni. We performed neutron scattering and magnetic susceptibility measurements in $La_{1.85}Sr_{0.15}Cu_{1-y}Zn_yO_4$ ($Zn: y=0.004, 0.008, 0.011, 0.017$) and $La_{1.85}Sr_{0.15}Cu_{1-y}Ni_yO_4$ ($Ni: y=0.009, 0.018, 0.029$).

II. SAMPLE PREPARATION AND EXPERIMENTAL DETAILS

Neutron scattering studies of spin excitations require large and spatially homogeneous single crystals due to weak signals. Moreover, for the study of the impurity effect, it is essential to control impurity concentrations correctly without changing other properties—for example, Sr concentration homogeneity and mosaicness. We controlled the size, shape, and growth direction of crystals for all samples in order to unify experimental conditions and realize the quantitative comparisons of results among different samples. characterization of crystals and unification of experimental conditions.

Single crystals of $La_{1.85}Sr_{0.15}CuO_4$, $La_{1.85}Sr_{0.15}Cu_{1-y}Zn_yO_4$ ($Zn: y=0.004$, 0.008, 0.011, 0.017), and $La_{1.85}Sr_{0.15}Cu_{1-y}Zn_yO_4$ ($Ni: y=0.009$, 0.018, 0.029) were grown using the traveling-solvent-floating-zone (TSFZ) method. Feed rods were prepared by the ordinary solid-state reaction method. Dried powders of La_2O_3, $SrCO_3$, CuO, ZnO, and NiO were weighed and mixed. The mixed powder was ground and calcined at 900 °C for 20 h for four times in air. After several grindings and calcinations of powder, we added extra CuO of 2 mol % into the powder in order to compensate the loss of Cu during the crystal growth. The powder was formed into a cylindrical rod and the rod, was hydrostatically pressed. We sintered the rod at 1250 °C for 24 h in air. The solvent material with a composition of $La:Sr:Cu:Zn(Ni)=1.85:0.15:(4\text{-}y):y$ for each y was prepared. We use 0.3 g of the solvent and a $La_{1.85}Sr_{0.15}Cu_{1-y}A_yO_4$ ($A=Zn, Ni$) single crystals as a seed rod. We controlled the growth direction of crystals by using the seed rod the direction of the cylinder of which is the a axis. The TSFZ operation was carried out using infrared image furnaces (NEC Machinery Co., SC-4 and SC-35HD) with small two halogen lamps and double ellipsoidal mirrors. To cut off reflections of the light from high angles, a silica tube was partially covered with aluminum foils. This yields a sharp temperature gradient in the direction of crystal growth, which helps to stabilize the melting zone. The growth rate was kept constant at 1.0 mm/h, and both the feed and seed rods were rotated 30 and 15 rpm, respectively. We flowed mixed gas of argon and oxygen with the flow rate of 100 cm^3/min ($Ar: 20\ cm^3/min, O: 80\ cm^3/min$). Crystal growth conditions for all the samples were kept same and we maintained the conditions for 100 h during crystal growth. After crystal growth, we put the crystal rod in water for 1 week to check the inclusion of La_2O_3 which reacts with water and changes to $La(OH)_3$. The appearance of $La(OH)_3$ breaks the crystal, because the molecular volume of $La(OH)_3$ is larger than that of La_2O_3. Finally, to eliminate oxygen deficiencies, all the crystals were annealed under oxygen gas flow at 900 °C for 50 h, cooled to 500 °C at a rate of 10 °C/h, and annealed at 500 °C for 50 h.

The concentrations of La, Sr, Cu, Zn, and Ni ions were precisely estimated by the inductively coupled plasma (ICP) analysis using Shimadzu ICPS-7500. Within the detection limit of the ICP analysis, no observable impurities were detected. We checked the spatial homogeneity of Sr, Zn, and Ni ions by comparing the values measurements for small portions of crystals taken at different points of each sample, and we confirm the macroscopic homogeneity of composition. The obtained values of Sr, Zn, and Ni concentrations are summarized in Table I. The values of Sr concentration for all the sample are $x\sim0.15$ within the measurement error, and those of impurity concentrations are substantially larger than the error. These results show that we could control the impurity doping rate with keeping the Sr concentration. We also determined the structural phase transition temperature T_{d1} by neutron diffraction measurement. As temperature decreases, the crystal structure changes from HTT to low-temperature orthorhombic (LTO) at T_{d1}. The $(072)_{ortho}$ superlattice peak in the LTO notation appears below T_{d1}, and we measured temperature dependence of the $(072)_{ortho}$ peak intensity. As seen in Table I, the obtained values of T_{d1} for all the samples are almost same and consistent with that of LSCO ($x=0.15$).[3] T_{d1} is very sensitive to the Sr concentration, and the T_{d1} reduction rate is $\sim 22K/x$ at. %. Hence, these results show that the Sr concentration for all samples is $x\sim0.15$ and Sr ions are doped homogeneously into the crystals. In the Zn-doped samples, T_{d1} becomes somewhat high with in-

TABLE I. Sr, Zn, and Ni concentrations estimated by ICP analysis and T_{d1} determined by netron diffraction in $La_{1.85}Sr_{0.15}Cu_{1-y}A_yO_4$ (A=Zn,Ni).

Sample	Sr x	Zn or Ni y	T_{d1}
y=0	0.142(8)	—	186 K
Zn:y=0.004	0.144(3)	0.0044(4)	
Zn:y=0.008	0.147(4)	0.0083(3)	192 K
Zn:y=0.011	0.144(7)	0.0112(5)	
Zn:y=0.017	0.145(2)	0.0170(7)	202 K
Ni:y=0.009	0.145(7)	0.0090(3)	
Ni:y=0.018	0.144(6)	0.0185(5)	184 K
Ni:y=0.029	0.142(6)	0.0287(8)	182 K

creasing the doping contents. On the other hand, T_{d1} of the Ni-doped samples is almost equal to that of the impurity-free sample. Gaojie *et al.* reported that the crystal structure of Zn-doped LSCO (x=0.15,Zn:$y \geqslant$0.15) is orthorhombic in room temperature, while that of Ni-doped LSCO (x =0.15,Ni:$y \leqslant$0.30) remains tetragonal.[18] Their results are consistent with our results; though Zn slightly increases T_{d1}, a small amount of impurities hardly affects the averaged crystal structure. inhomogeneity and concentration shift, Furthermore, we measured rocking curves of crystals by neutron diffraction. The full width half maximum (FWHM) is $\sim$0.15° for all samples, suggesting a good crystallinity.

Inelastic neutron scattering experiments were performed with the Tohoku University triple-axis spectrometer (TOPAN) installed at the JRR-3M reactor in the Japan Atomic Energy Research Institute (JAERI). The final energy was fixed at E_f=13.5 meV using the (002) reflection of a pyrolytic graphite analyzer. The horizontal collimator sequences were 40′-100′-*S*-60′-80′ (a low-resolution condition) and 40′-30′-*S*-30′-80′ (a high-resolution condition), where *S* denotes the sample position. A pyrolytic graphite filter and a sapphire filter were placed to reduce higher-order reflections and fast neutrons. To compare magnetic signals quantitatively, these experimental conditions were unified throughout the experiments. Elastic neutron scattering experiments were performed using TOPAN for Zn-doped sample and ISSP triple-axis spectrometer PONTA also in JRR-3M for Ni-doped sample. We selected the incident and final energies of 13.5 meV with the horizontal collimator sequence of 40′-30′-*S*-30′-80′ for the Zn-doped samples and 14.7 meV with 40′-40′-*S*-40′-80′ for the Ni-doped samples. In order to increase the sample volume, the columnar-shaped crystals (typical size of each crystal was 5 mm$\phi \times$25 mm) were assembled and mounted in the (hk0) zone. Since we controlled the growth axis parallel to the a axis, all the crystal arrangements were kept identical. In this paper, we denote the crystallographic indices by the HTT notation if no specification is given. The crystals were mounted in aluminum containers in which He gas was charged to act as a heat exchanger. ^{4}He closed-cycle refrigerators were used to cool the samples down to 4 K or 10 K for inelastic scattering measurements, and a top-loading liquid-^{4}He cryostat was used to cool down to 1.5 K for elastic measurements.

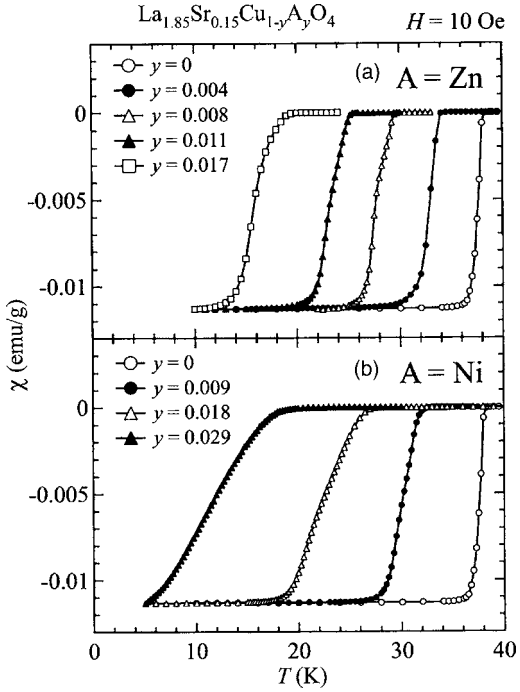

FIG. 1. Shielding signals of (a) $La_{1.85}Sr_{0.15}Cu_{1-y}Zn_yO_4$ (Zn:y =0,0.004,0.008,0.011,0.017) and (b) $La_{1.85}Sr_{0.15}Cu_{1-y}Ni_yO_4$ (Ni:y=0,0.009,0.018,0.029) measured under a magnetic field of 10 Oe. The values of susceptibility for all samples are scaled to $-1/4\pi$ (emu).

III. RESULTS

A. T_c suppression by impurity doping

To estimate the T_c reduction by impurity doping, we measured the magnetic susceptibilities under zero-field cooling using a superconducting quantum interference device (SQUID) magnetometer. Figure 1 shows the shielding signals of the impurity-doped LSCO samples, and the signals are scaled so that the transition widths ΔT_c are compared. We define T_c as the temperature at which the shielding signal is half of the low-temperature saturated value, and ΔT_c is defined as a difference between two temperatures where the signal is 10% and 90% of the low-temperature value. The values of T_c and ΔT_c are listed in Table II. The values of T_c

TABLE II. T_c and ΔT_c estimated by shielding signals.

Sample	T_c (midpoint)	ΔT_c
y=0	36.8 K	1.7 K
Zn:y=0.004	32.6 K	2.2 K
Zn:y=0.008	27.8 K	2.5 K
Zn:y=0.011	23.2 K	2.9 K
Zn:y=0.017	16.0 K	3.8 K
Ni:y=0.009	30.0 K	2.8 K
Ni:y=0.018	22.5 K	5.9 K
Ni:y=0.029	11.6 K	9.2 K

are in good agreement with those of previous studies,[10] and the reduction rates of T_c are 12.5 K/% for Zn and 8.7 K/% for Ni. In addition, ΔT_c is almost constant regardless of the Zn concentration, while ΔT_c broadens with increasing Ni.

One may consider that the broadening of T_c is caused by a spatial inhomogeneity of Ni concentration. As for Ni:y =0.029, we performed two measurements to investigate the inhomogeneity of Ni. First, we checked the concentration gradient of Ni along the growth or radial direction of cylindrical crystal, because we guess that the concentration gradient might occur along the two directions in the floating-zone method. radial direction of cylindrical crystal, We cut the crystal into several portions with the size of 1 mm^3 and evaluated the Ni concentration of each portion by ICP analysis. The obtained values are identical within the measurement error, and the error corresponds to ΔT_c of 2 K. The millimeter-sized inhomogeneity of Ni ions cannot account for the actual large ΔT_c (~9 K). Second, to check the microscopic inhomogeneity, we performed small-angle neutron scattering measurements using the T1-2 double-axis spectrometer attached to a thermal guide in JRR-3M, which is owned by IMR, Tohoku University. If clusters of Ni ions are produced in a CuO_2 plane, signals should appear in the small-angle region corresponding to a characteristic scale of the cluster size. However, no such signal was detected in the range $0.1 \leqslant Q \leqslant 1$ Å^{-1}. If signals appear below $Q=0.1$ Å^{-1}, one cluster contains Ni ions more than 30 and the mean distance between clusters exceeds 100 Å. This situation seems improper, because such a segregation should introduce two superconducting transition temperatures. As shown in Fig. 1, though the superconducting transition broadens, the temperature dependence show no two-step behavior. Besides, as listed in Table I, the structural transition temperature T_{d1} does not change by Ni doping. If clusters of Ni ions exist, the averaged crystal structure should be affected. Thus, we believe that there is no cluster of Ni in the crystal. These behaviors—the broadening of T_c and no change of T_{d1}—are consistent with results reported by Churei *et al.*[19] Moreover, crystal growth conditions for both Zn- and Ni-doped samples were kept same. Since the Zn-doped samples do not exhibit broadening of T_c, the broadening is a characteristic behavior to the Ni substitution. From these results, it is considered reasonable that Ni ions are introduced into the CuO_2 plane homogeneously and that the broadening of T_c is an intrinsic effect of Ni doping.

B. Energy spectra of spin excitations

Figure 2 shows constant-energy spectra of the spin excitations at $\omega=3$, 6, 8 meV for impurity-free $La_{1.85}Sr_{0.15}CuO_4$. The scan through two incommensurate peaks corresponds to the trajectory A illustrated at the top of Fig. 2. At 10 K, a clear spin gap was observed and is consistent with the previous studies.[3,4] In Figs. 3 and 4, we show Q profiles at ω =3,6,8 meV for Zn:y=0.004,0.008,0.0110.017 and Ni:y =0.009,0.018,0.029, measured below T_c (solid circles) and just above T_c (open circles). The trajectories of scans and experimental conditions are identical to those for impurity-free LSCO.

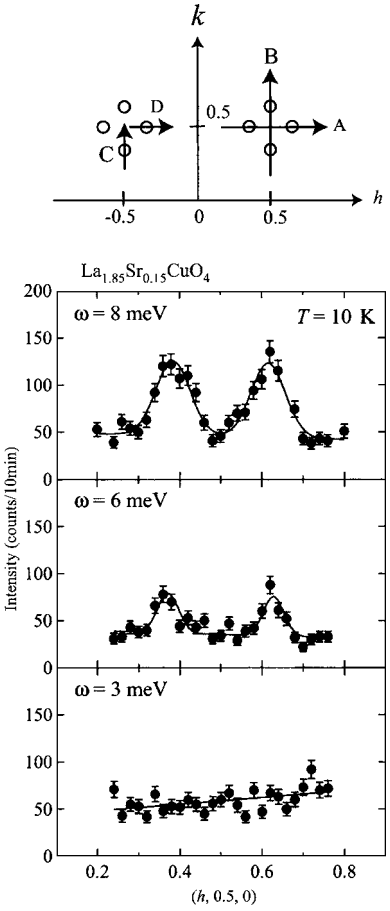

FIG. 2. (Top) Schematic drawing of scan trajectories. Open circles denote magnetic incommensurate peaks. (Bottom) Peak profiles along the h direction (trajectory A) for $La_{1.85}Sr_{0.15}CuO_4$ at ω =3, 6, and 8 meV. Solid lines are the result of fits with assuming two equivalent Gaussian peaks at $(0.5\pm\delta,0.5,0)$ and a linear background.

In Zn:y=0.004 and Ni:y=0.009, the spin excitations at ω=3 meV disappear at low temperatures, suggesting a spin-gap opening analogous to impurity-free LSCO, while in Zn:$y \geqslant 0.008$ and Ni:$y \geqslant 0.018$ the magnetic signals at ω =3 meV appear at low temperatures. These results suggest that both Zn and Ni dopings yield the low-energy spin excitations and the effect by Ni is weaker than that by Zn. In Ni:y=0.018 and Ni:y=0.029, as ω increases, the magnetic peak intensity increases and the peak width apparently broadens. The effect becomes marked with increasing Ni. On the other hand, Zn does not affect the peak profiles of spin excitations.

Figures 5 and 6 show energy spectra of the dynamical magnetic susceptibility $\chi''(Q_\delta,\omega)$ at the peak position Q =Q_δ below T=10 K for both the Zn- and Ni-doped samples. The open circles and solid lines in the figures denote $\chi''(Q_\delta,\omega)$ for impurity-free LSCO. Here $\chi''(Q,\omega)$ corresponds to the dynamical structure factor $S(Q,\omega)$ corrected with the thermal population factor,

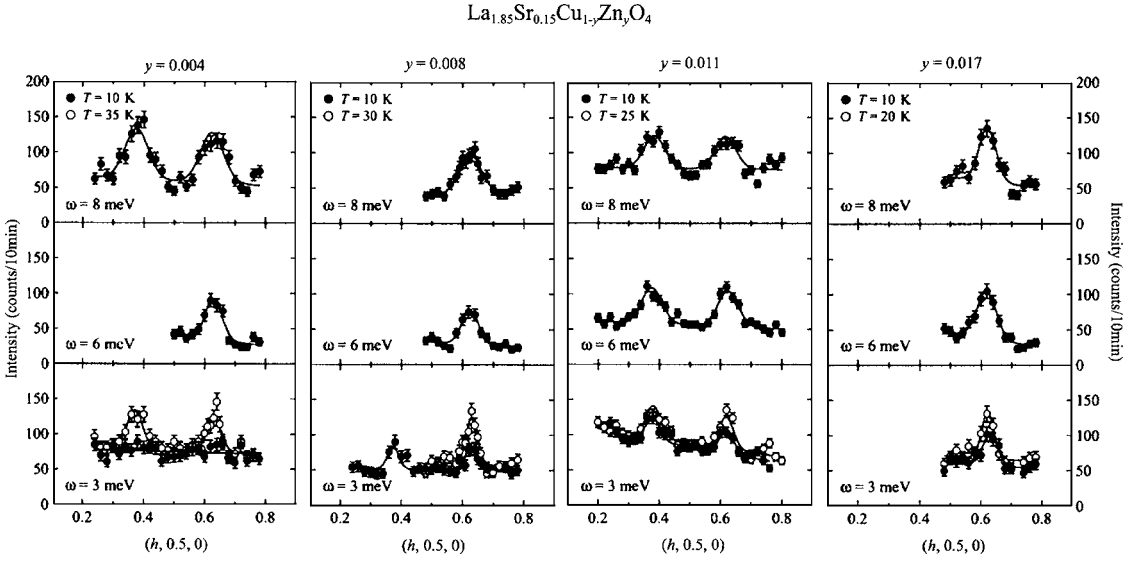

FIG. 3. Peak profiles along the h direction (trajectory A in Fig. 2) for $La_{1.85}Sr_{0.15}Cu_{1-y}Zn_yO_4$ (Zn: $y=0.004, 0.008, 0.011, 0.017$) at $\omega=3$, 6, and 8 meV. Solid and open circles correspond to the data below and above T_c. Solid lines are the fitting results by a Gaussian function with assuming two equivalent Gaussian peaks at $(0.5\pm\delta, 0.5, 0)$ and a linear background. We show the intensities divided by 2 for Zn: $y=0.011$, because the volume of sample with Zn: $y=0.011$ is approximately twice as large as those of the other Zn-doped samples.

$$S(Q,\omega)=\frac{1}{1-e^{-\hbar\omega/k_BT}}\chi''(Q,\omega). \quad (1)$$

Magnetic signals are fitted to Gaussian peaks in Figs. 3 and 4. We have estimated $S(Q_\delta,\omega)$ from the fitted peak amplitude corrected by taking account of the presence of higher-harmonics neutrons in the incident beam. The error bars in Figs. 5 and 6 are correspond to the fitting error. We also normalize the estimated $\chi''(Q_\delta,\omega)$ by the intensity of transverse acoustic phonons at $(2,-0.19,0)_{ortho}$ which should be proportional to the effective sample volume.

In the impurity-free sample, $\chi''(Q_\delta,\omega)$ monotonically decreases below $\sim$8 meV ($\equiv\omega_{sg}$), reflecting the gap structure. As for Zn doping, excitations in $\omega\leqslant\omega_{sg}$ increase, while $\chi''(\omega_{sg})$ is almost unchanged. These results show that additional low-energy spin excitations are induced by Zn doping. As Zn increases, the excitations appear in the lower-energy region due to the development of the additional state.

$\chi''(Q_\delta,\omega)$ of Ni: $y=0.009$ shows a behavior similar to that of Zn: $y=0.004$; though the low-energy excitations appear below ω_{sg}, the spin gap still opens. In Ni: $y=0.018$, the low-energy spin excitations are observable at $\omega=3$ meV, but the excitations below $\omega=2$ meV disappear. The spin excitations above 2 meV are observed in Ni: $y=0.029$, showing a tendency of gap closing. One of the most remarkable results is that the amplitude of $\chi''(Q_\delta,\omega)$ for Ni: $y=0.018$ and Ni: $y=0.029$ is much larger than that for $y=0$ and Ni: $y=0.009$.

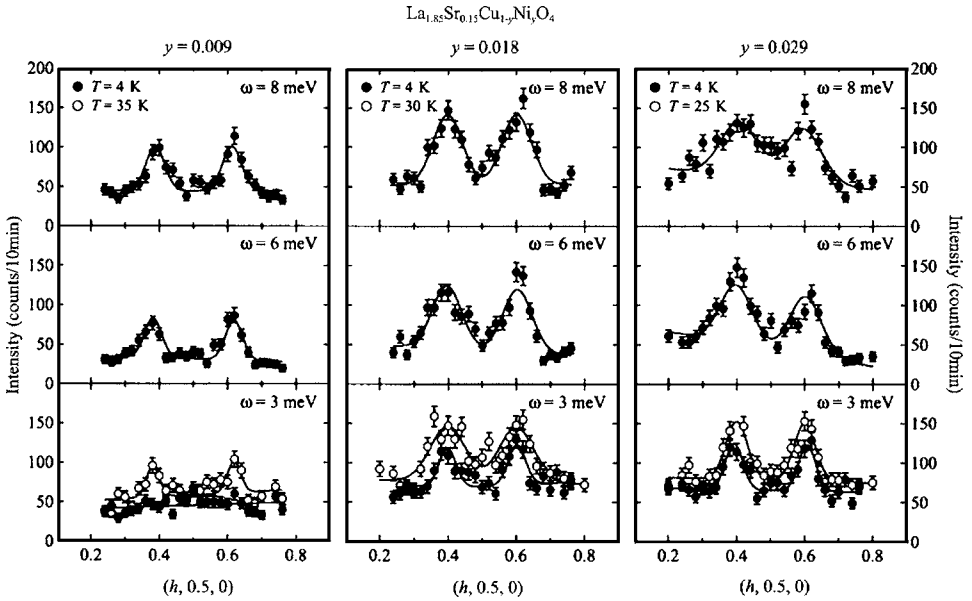

FIG. 4. Peak profiles along the h direction (trajectory A in Fig. 2) for $La_{1.85}Sr_{0.15}Cu_{1-y}Ni_yO_4$ (Ni: $y=0.009, 0.018, 0.029$) at $\omega=3$, 6, and 8 meV. Solid and open circles correspond to the data below and above T_c. Solid lines are the fitting results assuming two equivalent Gaussian peaks at $(0.5\pm\delta, 0.5, 0)$ and a linear background.

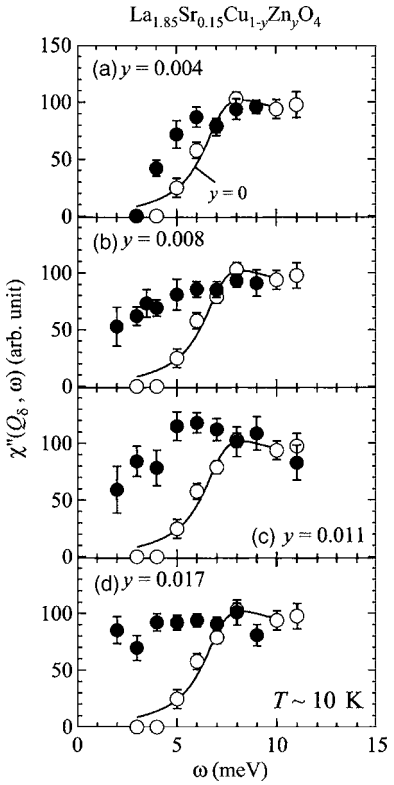

FIG. 5. Energy dependence of $\chi''(Q_\delta, \omega)$ for $La_{1.85}Sr_{0.15}Cu_{1-y}Zn_yO_4$ with (a) Zn: y=0.004, (b) Zn: y=0.008, (c) Zn: y=0.011, and (d) Zn: y=0.017 at $T \sim 10$ K. Open circles are the data for the impurity-free sample, and solid lines are guides to the eye.

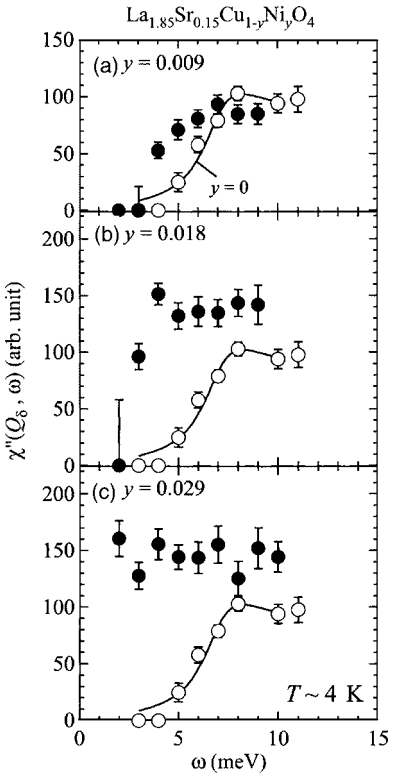

FIG. 6. Energy dependence of $\chi''(Q_\delta, \omega)$ for $La_{1.85}Sr_{0.15}Cu_{1-y}Ni_yO_4$ with (a) Ni: y=0.009, (b) Ni: y=0.018, and (c) Ni: y=0.029 at $T \sim 4$ K. Open circles are the data for the impurity-free sample, and solid lines are guides to the eye.

C. Temperature dependence of spin excitations

The temperature dependence of $\chi''(Q_\delta, \omega)$ at ω=3 meV is shown in Fig. 7 for the Zn-doped samples. $\chi''(Q_\delta, \omega)$ of Zn: y=0.004 decreases below T_c, suggesting a gap opening similar to the impurity-free sample. In Zn: y=0.008 and Zn: y=0.011, the magnetic signal once starts decreasing around T_c, which also suggests the gap opening. However, the signal increases again at lower temperature, indicating an emergence of the additional state. Figure 8 presents peak profiles of Zn: y=0.011 at T=10 K, 15 K and 20 K. Apparently, the peak intensity at T=15 K is smaller than those at T=10 and 20 K. This upturn behavior indicates two components of the spin excitations, and we regard them as an additive state and the spin-gap state. We consider that the low-energy additive state is not caused by the gap shift or broadening and that it is a novel spin state induced by Zn. Here we call the novel state an *in-gap* state, as defined by Kimura *et al.*[15,16] The temperature which the signals begin to decrease in Zn: y=0.011 is lower than that in Zn: y=0.008, suggesting that the temperature of gap opening is associated with T_c. In Zn: y=0.017, $\chi''(Q_\delta, \omega)$ shows no temperature dependence, implying the reduction of spin-gap energy and the development of the in-gap state.

In Fig. 9, we show the temperature dependence of $\chi''(Q_\delta, \omega)$ at ω=3 meV for the Ni-doped samples. In Ni: y =0.009, $\chi''(Q_\delta, \omega)$ decreases below T_c, suggesting a gap opening. $\chi''(Q_\delta, \omega)$ of Ni: y=0.018 shows no upturn as opposed to those of Zn: y=0.008 and Zn: y=0.011, which indicates the absence of the in-gap state. Thus, in the Ni-doped samples, the spin gap simply closes with increasing Ni, which is not caused by the development of the in-gap state but by the gap shift or broadening.

D. Q-ω dependence of incommensurate peaks

In order to investigate the impurity effects on the magnetic peak profile in more detail, we performed inelastic neutron scattering measurements under a high-resolution condition. Figure 10 shows peak profiles at ω=8 meV for the impurity-free, the Zn-doped with Zn: y=0.017, and the Ni-doped with Ni: y=0.029 samples, taken at 11 K, 4 K, and 4 K, respectively. In Zn: y=0.017, clear incommensurate magnetic peaks were observed, and the peak width and position are almost identical to those of impurity-free sample. In contrast, the magnetic peak width broadens in Ni: y =0.029 and the peak position shifts toward the magnetic zone center (0.5, 0.5, 0). In Fig. 11, we plot the q-ω dependence of the peak position for the impurity-free, the Zn-doped (Zn: y=0.011,0.017), and the Ni-doped (Ni: y =0.018,0.029) samples. Shaded regions represent the FWHM of incommensurate magnetic peaks, and a dashed line shows the peak positions for the impurity-free sample. In the impurity-free sample, the peak positions and widths are independent of the excitation energy. The peak positions

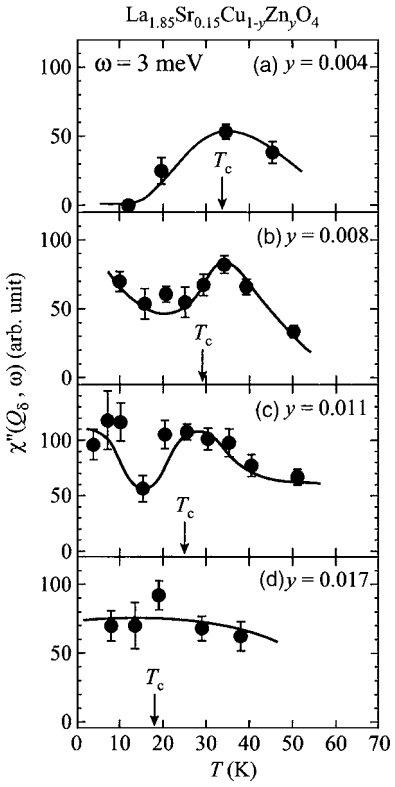

FIG. 7. Temperature dependence of $\chi''(Q_\delta,\omega)$ for $La_{0.85}Sr_{0.15}Cu_{1-y}Zn_yO_4$ with (a) Zn:y=0.004, (b) Zn:y=0.008, (c) Zn:y=0.011, and (d) Zn:y=0.017 at ω=3 meV. $\chi''(Q,\omega)$ denote the fitted peak amplitude corrected with the thermal population factor. Solid lines are guides to the eye, and arrowheads indicate the onset values of T_c.

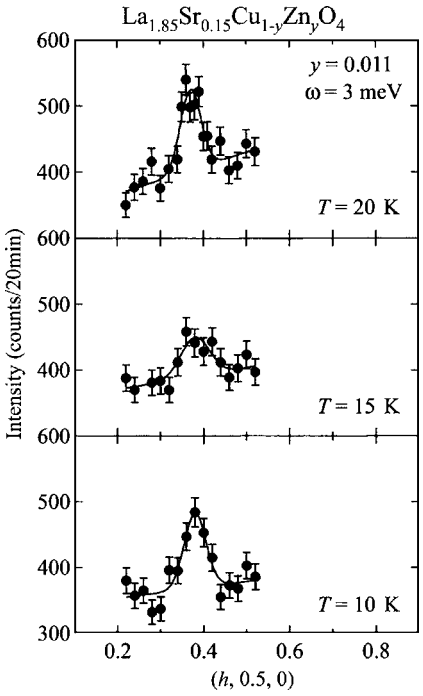

FIG. 8. Peak profiles along the h direction (trajectory A in Fig. 2) for $La_{1.85}Sr_{0.15}Cu_{1-y}Zn_yO_4$ (Zn:y=0.011) at T=10, 15, and 20 K. All the data were taken at ω=3 meV. Solid lines are the fitting results assuming a Gaussian peak and a linear backgound.

and widths of the Zn-doped samples almost coincide with those of the impurity-free sample, while in the Ni-doped samples, as the excitation energy increases, the peak positions apparently deviate from the dashed line and approach q=0. Furthermore, the peak broadens more drastically with increasing energy. These results suggest that the spin excitations of Ni-doped samples are dispersive and broaden with increasing energy. These phenomena are characteristic of Ni and become marked with increasing the doping concentration.

E. Elastic scattering

We performed elastic scattering measurements for Zn:y =0.017 and Ni:y=0.029. Figure 12 shows the peak profiles at T=1.5 and 40 K and the temperature dependence of the elastic peak intensity. In Zn:y=0.008 and Zn:y=0.011, there is no observable signal, suggesting that the spin gap still opens. However, a very sharp peak was clearly observed in Zn:y=0.017 at T=1.5 K and the signals appear below T ~20 K. On the other hand, in the Ni-doped LSCO, we found a broader peak, which shows no temperature dependence. Recently, Hiraka and co-workers have reported that no clear elastic peak was detected while a peak was observed at ω =0.4 meV for $La_{1.85}Sr_{0.15}Cu_{1-y}Ni_yO_4$ (y=0.02), with the instrumental energy resolution of ~0.2 meV.[19,20] In our case, the instrumental resolution is ~1.2 meV, and we consider that the observed "elastic" peaks arise from the inelastic components which are detected due to a broad energy resolution. sample. We discuss these elastic signals from the viewpoint of spectral weight shift of spin excitation in Sec. IV A 2.

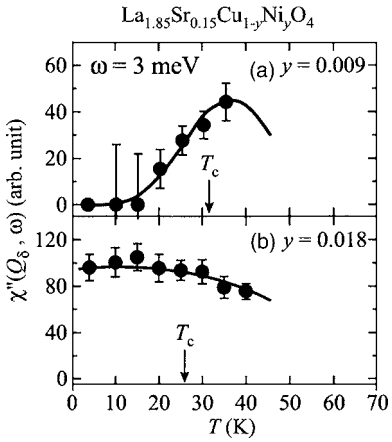

FIG. 9. Temperature dependence of $\chi''(Q_\delta,\omega)$ for $La_{1.85}Sr_{0.15}Cu_{1-y}Ni_yO_4$ with (a) Ni:y=0.009 and (b) Ni:y=0.018 at ω=3 meV. $\chi''(Q,\omega)$ denotes the fitted peak amplitude corrected with the thermal population factor. Solid lines are guides to the eye, and arrowheads indicate the onset values of T_c.

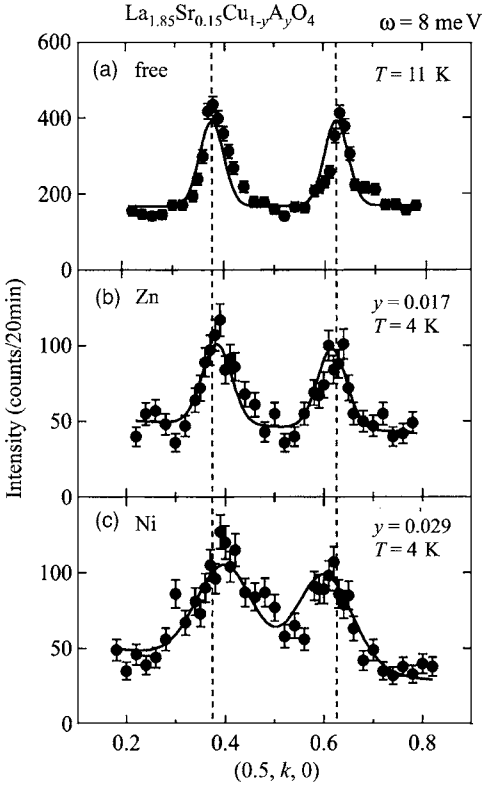

FIG. 10. Q profiles along the k direction (trajectory B in Fig. 2) for (a) $La_{1.85}Sr_{0.15}CuO_4$, (b) $La_{1.85}Sr_{0.15}Cu_{1-y}Zn_yO_4$ (Zn: $y=0.017$), and (c) $La_{1.85}Sr_{0.15}Cu_{1-y}Ni_yO_4$ (Ni: $y=0.029$) at $\omega=8$ meV under the high-resolution condition. These data were taken at low temperature. Solid lines are the result of fits with assuming two equivalent Gaussian peaks at $(0.5, 0.5\pm\delta, 0)$. Vertical dashed lines denote peak positions for (a) $La_{1.85}Sr_{0.15}CuO_4$ estimated by fitting.

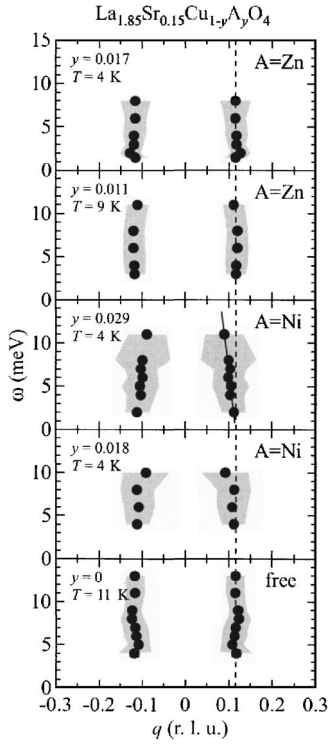

FIG. 11. Spin excitations for $y=0$, $La_{1.85}Sr_{0.15}Cu_{1-y}Zn_yO_4$ (Zn: $y=0.011, 0.017$) and $La_{1.85}Sr_{0.15}Cu_{1-y}Ni_yO_4$ (Ni: $y=0.018, 0.029$), at low temperature. q denotes the propagation vector of spin correlation; $q=0$ means the magnetic zone center $Q=(0.5, 0.5, 0)$. Solid circles and shaded regions represent the peak position and FWHM of incommensurate magnetic signals estimated from curve fitting. Dashed lines show a mean value of peak positions for the impurity-free sample. A solid line indicates a guide to the eye of dispersion for Ni: $y=0.029$.

IV. DISCUSSION

A. Differences between Zn and Ni doping effects

1. Dynamical feature

There are differences between Zn and Ni doping effects on spin excitations. One is the existence of upturn behavoir. In Zn: $y=0.008$ and Zn: $y=0.011$, we observed the upturn behavior in the temperature dependence of $\chi''(Q_\delta, \omega)$ at $\omega=3$ meV. This result suggests the existence of two components: an in-gap state and a spin-gap state. On the other hand, there is no upturn for Ni doping, indicating the absence of an in-gap state.

The other is a change of the q-ω structure of spin excitations. As for the spin-gap state in Zn-doped LSCO, the gap slightly moves to the lower energy, but q profiles of spin excitations are almost unchanged. This indicates that Zn has less effect on the spin-gap state. In the case of Ni doping, we did not observe evidence for the in-gap state. However, Ni changes spin excitations drastically: The spin gap shifts and broadens, and moreover, χ'' is enhanced and the spin excitations become dispersive. This suggests that Ni strongly affects the spin-gap state.

2. Feature near $\omega=0$

Zn induces a very sharp elastic peak below $T\sim 20$ K, and the signal exponentially increases with decreasing temperature. From previous neutron scattering studies in LSCO and related compounds, all observed elastic magnetic signals appear at low temperature and have sharp line width in the q direction.[21] This behavior is consistent with our results. Hirota *et al.* reported that Zn doping of $y=0.012$ shifts the spectral weight of the spin excitations from the inelastic to the quasielastic region at low temperature.[21,22] We consider that the increase of elastic signal at low temperature is owing to the spectral-weight shift resulting from the development of the in-gap state. In other words, the static component arises from the in-gap state which is stabilized at low temperature.

We found a broad peak which shows no temperature dependence in Ni-doped LSCO. We mentioned in Sec. III E that the elastic signals in the Ni doping case involve inelastic components because of the coarse energy resolution. Furthermore, as discussed above, no upturn bahavior indicates the absence of in-gap state. Combining these facts, we thus conclude that the static component does not exist in the Ni-doped sample.

3. Superconducting state

Ni strongly affects not only the spin-gap state but also the superconducting transition unlike Zn doping. The transition

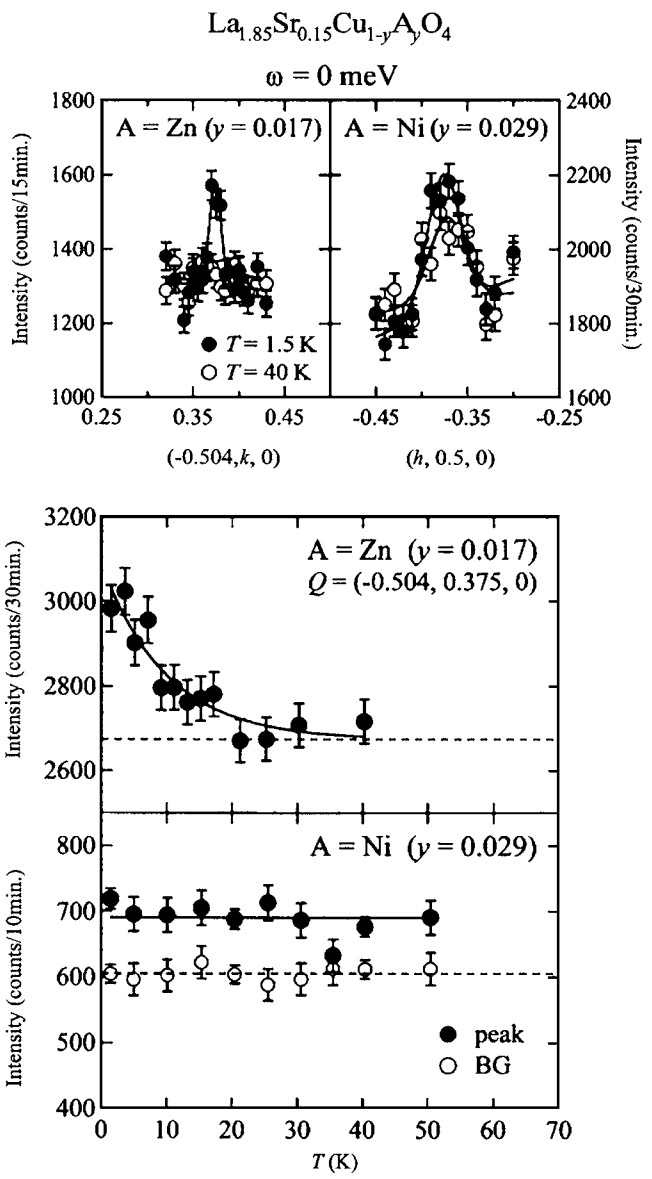

FIG. 12. The incommensurate elastic peak intensities as a function of temperature for $La_{1.85}Sr_{0.15}Cu_{1-y}Zn_yO_4$ (Zn: $y=0.017$) and $La_{1.85}Sr_{0.15}Cu_{1-y}Ni_yO_4$ (Ni: $y=0.029$). The top figures show q profiles along (a) the k direction (trajectory C in Fig. 2) for the Zn-doped sample and (b) the h direction (trajectory D in Fig. 2) for the Ni-doped sample at 1.5 and 40 K. Solid lines represent the result of fits by a Gaussian function. (c) Temperature dependence of intensity at the peak position $Q=(-0.504,0.375,0)$ for the Zn-doped sample. Solid and dashed lines are guides to the eye and estimated backgrounds. (d) Temperature dependence of peak (solid circles) and background (open circles) intensities for the Ni-doped sample. Peak intensity corresponds to the average of intensity at $Q=(-0.37,0.5,0)$, $(-0.38,0.5,0)$, and $(-0.39,0.5,0)$, and background intensity corresponds to the average of intensity at $Q=(-0.32,0.5,0)$ and $(-0.44,0.5,0)$. Solid and dashed lines are guides to the eye of peak and background.

width ΔT_c is almost constant as a function of the Zn concentration, while ΔT_c broadens with increasing Ni. It seems that the effects on the spin-gap state are associated with the change of the electronic state of the superconductivity.

4. Inhomogeneous picture

For impurity-doped systems, spatially inhomogeneous pictures have been proposed[17,23,24]; impurities make the nonsuperconducting *island* with radius ξ in the superconducting *sea* and induce local moments in the island. Our results revealed that the magnetic excitations in Zn-doped LSCO consist of two components: the spin-gap state and in-gap state. Combining these results, we thus consider that the superconducting sea gives the spin-gap state and the coherence between the local moments inside the nonsuperconducting island results in the in-gap state. In our speculation, the coherence of local moments is connected across the superconducting sea, which we call an *interisland* correlation. We discuss in detail this correlation in Sec. IV B.

In Ni-doped LSCO, we observed no evidence for the in-gap state. μSR studies and uniform susceptibility measurements suggest that Ni also induces local moments in a nonsuperconducting island similar to Zn.[10,23–26] However in these studies, the estimated value of radius ξ induced by Ni is smaller than the case of Zn doping. In the case of Ni doping, therefore, it is considered that the interisland correlation extends not enough to be detected by neutron scattering due to small ξ. lower temperature appear at a lower temperature Thus, we conclude that the in-gap state is invisible and that we only observed the spin state of superconducting sea in the case of Ni doping.

We schematically show our concept in Fig. 13 from a viewpoint of the inhomogeneous picture. Zn induces nonsuperconducting islands and hardly affects the superconducting sea, so that the spin-gap state and ΔT_c are almost unchanged. On the contrary, Ni primarily influences the sea. In other word, Ni affects the electronic and magnetic states of the superconductivity, leading to the modified spin-gap state and the broadening of ΔT_c.

B. Zn doping effects: The in-gap state

A primary effect by Zn on the spin excitations is the appearance of an in-gap state. The most obvious evidence for the in-gap state is the upturn in the temperature dependence of $\chi''(Q_\delta,\omega)$ at $\omega=3$ meV. Previously Kimura *et al.* reported the upturn behavior in Zn: $y=0.008$.[15,16] In the present study, we also confirmed the upturn behavior in Zn: $y=0.011$. In $YBa_2(Cu_{1-y}Zn_y)_3O_{6.97}$ ($y=0.02$), similar results have been reported by Sidis *et al.*[27] Their inelastic neutron scattering measurements showed that magnetic signals emerge around $\omega\sim 9$ meV while the spin gap is retained and that χ'' at $\omega=10$ meV is almost temperature independent below T_c. Their results indicate the coexistence of the in-gap state with the spin-gap state at low temperature, signifying that the appearance of in-gap state is a universal phenomenon in Zn-doped high-T_c cuprates. Note that the in-gap state appears at the same Q position as that of the normal and high-energy states for both LSCO and YBCO. Therefore, Zn locally slows spin fluctuations without modifying the AF wave vector. In other words, Zn seems to act as a pinning center of AF spin fluctuations.

As for Zn: $y=0.017$, the in-plane static spin correlation length ξ_{ab} ($\sim$80 Å) is much longer than $R_{\text{Zn-Zn}}$ ($\sim$29 Å)

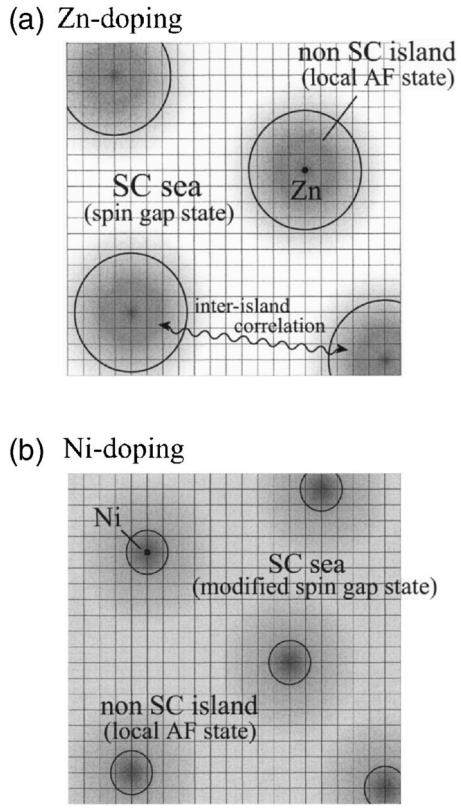

FIG. 13. Schematic drawing of an inhomogeneous mixture of the superconducting (SC) sea with the spin-gap state and the nonsuperconducting islands with the local AF correlation. (a) and (b) correspond to the cases of Zn doping and Ni doping. Refer to the text for the meaning of interisland correlation and modified spin-gap state.

which corresponds to the mean distance between the nearest-neighbor Zn ions. These results indicate that the spin correlations of the in-gap state do not result from the local AF coherence in an individual island, but from the interisland correlation among islands, which is schematically shown in Fig. 13(a). One may argue that it is caused by an overlap of islands. However, our results show the coexistence of the spin-gap and in-gap states (see Fig. 7), suggesting a phase separation of islands and sea in nanolength scale. Therefore we conclude that induced moments in the nonsuperconducting island correlate with those in spatially separated islands beyond the superconducting sea.

C. Threshold in Ni doping effects

We observed that the amplitude of $\chi''(Q_\delta,\omega)$ for Ni:$y=0.018$ and Ni:$y=0.029$ is much larger than that for $y=0$ and Ni:$y=0.009$, signifying that there exists a certain threshold between Ni:$y=0.009$ and Ni:$y=0.018$. We speculate that the threshold corresponds to a critical Ni concentration y_0 where the valence of Ni ions changes; Nakano *et al.* have reported that no Curie term appears in the uniform susceptibility measurements below the critical Ni concentration y_0.[26] They also reported that the characteristic temperature which χ exhibits a broad peak, so-called T_{max}, increases with increasing Ni below y_0. On the other hand, the Curie term appears and T_{max} does not change above y_0. If the valence of Ni ions are not divalent, the effective hole concentration p should change, leading to the variation of T_{max} which is susceptible to p. From these results, they conclude that Ni ions are substituted for Cu ions as Ni^{3+} ($S=1/2$: low-spin state) below y_0 and Ni^{2+} ($S=1$) above y_0; Ni^{3+} has the spin of $S=1/2$ as well as that of Cu^{2+}, indicating that the Ni^{3+} substitution hardly affects the spin correlation in the CuO_2 plane. In our result, $\chi''(Q_\delta,\omega)$ of Ni:$y=0.009$ is almost same as that of $y=0$ except for a slight gap broadening. This behavior of Ni:$y=0.009$ is consistent with the absence of the Curie term and the reduction of p below y_0 (~ 0.01 for $x=0.15$). In this argument, it is also considered that that the enhancement of $\chi''(Q_\delta,\omega)$ for Ni:$y=0.018$ and Ni:$y=0.029$ is a characteristic effect of the magnetic impurity with $S=1$ spin.

D. Spin excitations: A possible scaling with T_c

Recently, similarities of detailed q structure of spin excitations are discussed in YBCO (Ref. 28) and $La_{2-x}Ba_xCuO_4$ (LBCO) (Ref. 29): The low-energy spin excitations form incommensurate peaks, and the peaks disperse inwards toward Q_{AF}. At a characteristic energy, which is called E_r in YBCO, the peak is found at a commensurate position $Q=Q_{AF}$. In the higher-energy region, the excitations disperse outwards and form a square-shaped continuum. Furthermore, the dispersive excitations at low energy are observed in LSCO ($x=0.16$),[9] though the commensurate peak and the dispersion in the higher-energy region are not yet confirmed. These results suggest that such dispersive excitations are universal in the high-T_c cuprates. Quite surprisingly, the present results in Ni-doped samples show that the spin excitations are dispersive and broaden with increasing energy even in the low-energy region below 11 meV. These behaviors are very similar to those of impurity-free LSCO,[9] when the energy scale of spin excitations is adjusted. We plot the dispersion of spin excitations scaled to T_c as shown in Fig. 14. This q-ω plot indicates that Ni reduces the energy scale of spin excitations which associates with T_c. In addition, we recognize that the enhancement of χ'' in Ni-doped LSCO ($y \geqslant 0.018$) is also caused by the reduction of the energy scale of spin excitations. A previous neutron scattering study of YBCO reported that Ni reduces E_r with conserving the ratio E_r/T_c, while such a shift is much smaller in the Zn-doped sample.[30] Furthermore, a Cu NQR study of Ni-doped YBCO has shown that all the $1/T_1$ data in the normal state are on a universal curve when $1/T_1$ is plotted against $t=T/T_c$. Since $1/T_1$ is related to $\chi''(Q,\omega)$, the universality of $1/T_1$ implies that AF spin fluctuations are scaled to T_c upon Ni doping.[31] These results are consistent with our results, and we consider that these behaviors are consequences of the reduction of energy scale of spin excitations by Ni. However, at present, we cannot affirm how precisely the spin excitations are scaled to T_c, because we measured in the narrow energy region ($\omega \leqslant 11$ meV). Further inelastic neutron scattering studies in the higher-energy region are strongly required.

V. CONCLUSION

We have revealed the impurity effects on low-energy spin excitations in high-T_c cuprates. Zn doping induces local mo-

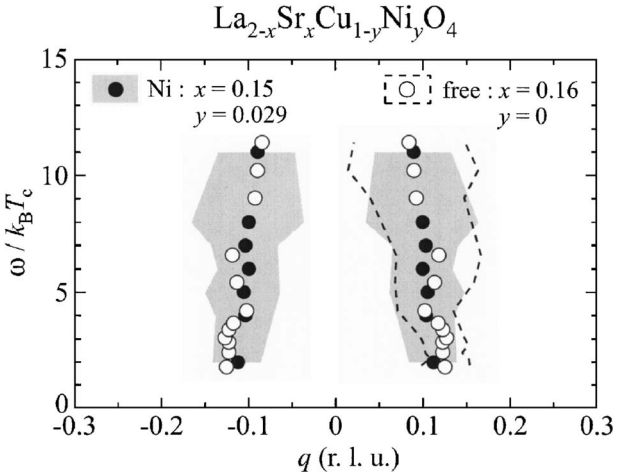

FIG. 14. Dispersions of spin excitations scaled by $k_B T_c$ for $La_{1.85}Sr_{0.15}Cu_{1-y}Ni_yO_4$ (Ni: $y=0.029$) at 4 K and $La_{1.84}Sr_{0.16}CuO_4$ (free: $x=0.16$) at 10 K (Ref. 9). q denotes the propagation vector of spin correlation. Solid (open) circles and shaded (dashed) regions represent the peak position and FWHM for Ni: $y=0.029$ (free: $x=0.16$), respectively.

ments within individual nonsuperconducting islands, and the islands are spatially separated from the superconducting sea, which is hardly affected by Zn. At low temperature, the local moments among different islands correlate, leading to the emergence of an in-gap state. The in-gap state appears at the same Q position in the normal and high-energy states, and Zn seems to act as a pinning center of AF spin fluctuations. We consider that Zn reduces the volume fraction of the superconducting regions, which results in the reduction of T_c.

We observed no evidence for the in-gap state in the case of Ni doping. We consider that the invisibility of the in-gap state arises from undeveloped spin correlations among different islands, because the islands are smaller than those of Zn doping. Instead, Ni primarily effects on the superconducting sea; the spin gap shifts or broadens, and Ni makes the spin excitations get broader and dispersive. These behaviors are recognized as a consequence of the reduction of energy scale of spin excitations. We believe that the reduction of energy scale is relevant to the suppression of T_c.

ACKNOWLEDGMENTS

We are grateful to M. Matsuura for experimental supports and critical discussions throughout the project. We are indebt to S. Hosoya and M. Onodera for technical help in the crystal growth. Neutron scattering experiments were supported by T. Asami, Y. Kawamura, K. Nemoto, K. Ohoyama, and S. Watanabe. We also thank T. Adachi, T. Churei, Y. Endoh, M. Fujita, H. Hiraka, K. Ishida, Y. Itoh, K. Iwasa, C. H. Lee, M. Matsuda, Y. Murakami, Y. Noda, and K. Yamada for stimulating discussions. This work was supported in part by a Grant-In-Aid for Scientific Research (B) (No. 15340109, 2003-2004) and a Grant-In-Aid for Encouragement of Young Scientist (No. 13740198, 2001-2002) from the Ministry of Education, Culture, Sports, Science and Technology of Japan.

*Present address: Institute of Materials Structure Science, KEK, Tsukuba 305-0801, Japan. Electronic address: kofu@post.kek.jp

[1] J. Rossat-Mignod, L. P. Legnault, P. Bourges, P. Burlet, C. Vettier, and J. Y. Henry, Physica B **192**, 109 (1993).
[2] C. H. Lee, K. Yamada, H. Hiraka, C. R. Venkateswara Rao, and Y. Endoh, Phys. Rev. B **67**, 134521 (2003).
[3] K. Yamada, S. Wakimoto, G. Shirane, C. H. Lee, M. A. Kastner, S. Hosoya, M. Greven, Y. Endoh, and R. J. Birgeneau, Phys. Rev. Lett. **75**, 1626 (1995).
[4] C. H. Lee, K. Yamada, Y. Endoh, G. Shirane, R. J. Birgeneau, M. A. Kastner, M. Greven, and Y.-J. Kim, J. Phys. Soc. Jpn. **69**, 1170 (2000).
[5] P. Dai, H. A. Mook, R. D. Hunt, and F. Doğan, Phys. Rev. B **63**, 054525 (2001).
[6] K. Yamada, C. H. Lee, K. Kurahashi, J. Wada, S. Wakimoto, S. Ueki, H. Kimura, Y. Endoh, S. Hosoya, G. Shirane, R. J. Birgeneau, M. Greven, M. A. Kastner, and Y. J. Kim, Phys. Rev. B **57**, 6165 (1998).
[7] M. Itoh, Y. Yasui, S. Iikubo, M. Soda, A. Kobayashi, M. Sato, K. Kakuai, C.-H. Lee, and K. Yamada, J. Phys. Soc. Jpn. **73**, 991 (2004).
[8] J. M. Tranquada, C. H. Lee, K. Yamada, Y. S. Lee, L. P. Regnault, and H. M. Rønnow, Phys. Rev. B **69**, 174507 (2004).
[9] N. B. Christensen, D. F. McMorrow, H. M. Rønnow, B. Lake, S. M. Hayden, G. Aeppli, T. G. Perring, M. Mangkorntong, M. Nohara, and H. Takagi, Phys. Rev. Lett. **93**, 147002 (2004).
[10] G. Xiao, M. Z. Cieplak, J. Q. Xiao, and C. L. Chien, Phys. Rev. B **42**, 8752 (1990).
[11] A. V. Mahajan, H. Alloul, G. Collin, and J. F. Marucco, Phys. Rev. Lett. **72**, 3100 (1994).
[12] M.-H. Julien, T. Fehér, M. Horvatić, C. Berthier, O. N. Bakharev, P. Ségransan, G. Collin, and J.-F. Marucco, Phys. Rev. Lett. **84**, 3422 (2000).
[13] S. H. Pan, E. W. Hudson, K. M. Lang, H. Eisaki, S. Uchida, and J. C. Davis, Nature (London) **403**, 746 (2000).
[14] E. W. Hudson, K. M. Lang, V. Madhavan, S. H. Pan, H. Eisaki, S. Uchida, and J. C. Davis, Nature (London) **411**, 920 (2001).
[15] H. Kimura, M. Kofu, Y. Matsumoto, and K. Hirota, Phys. Rev. Lett. **91**, 067002 (2003).
[16] H. Kimura, Physica C **392–396**, 34 (2003).
[17] B. Nachumi, A. Keren, K. Kojima, M. Larkin, G. M. Luke, J. Merrin, O. Tchernyshov, Y. J. Uemura, N. Ichikawa, M. Goto, and S. Uchida, Phys. Rev. Lett. **77**, 5421 (1996).
[18] X. Gaojie, M. Zhiqiang, T. Mingliang, W. Yu, and Z. Yuheng, J. Supercond. **10**, 13 (1997).
[19] T. Churei, H. Hiraka, Y. Endoh, M. Matsuda, and K. Yamada, Physica C **392–396**, 194 (2003).
[20] H. Hiraka, T. Churei, Y. Endoh, M. Matsuda, and K. Yamada, Physica C **408–410**, 775 (2004).
[21] K. Hirota, Physica C **357–360**, 61 (2001).

[22] K. Hirota, K. Yamada, I. Tanaka, and I. Kojima, Physica B **241–243**, 817 (1998).
[23] T. Adachi, S. Yairi, K. Takahashi, Y. Koike, I. Watanabe, and K. Nagamine, Phys. Rev. B **69**, 184507 (2004).
[24] T. Adachi, S. Yairi, Y. Koike, I. Watanabe, and K. Nagamine, Phys. Rev. B **70**, 060504(R) (2004).
[25] J. M. Terascon, L. H. Greene, P. Barboux, W. R. McKinnon, G. W. Hull, T. P. Orlando, K. A. Delin, S. Foner, and J. E. J. McNiff, Phys. Rev. B **36**, 8393 (1987).
[26] T. Nakano, N. Momono, T. Nagata, M. Oda, and M. Ido, Phys. Rev. B **58**, 5831 (1998).
[27] Y. Sidis, P. Bourges, B. Hennion, L. P. Regnault, R. Villeneuve, G. Collin, and J. F. Marucco, Phys. Rev. B **53**, 6811 (1996).
[28] S. M. Hayden, H. A. Mook, P. Dai, T. G. Perring, and F. Doğan, Nature (London) **429**, 531 (2004).
[29] J. M. Tranquada, H. Woo, T. G. Perring, H. Goka, G. D. Gu, G. Xu, M. Fujita, and K. Yamada, Nature (London) **429**, 534 (2004).
[30] Y. Sidis, P. Bourges, H. F. Fong, B. Keimer, L. P. Regnault, J. Bossy, A. Ivanov, B. Hennion, P. Gautier-Picard, G. Collin, D. L. Millius, and I. A. Aksay, Phys. Rev. Lett. **84**, 5900 (2000).
[31] Y. Tokunaga, K. Ishida, Y. Kitaoka, and K. Asayama, Solid State Commun. **103**, 43 (1997).